Supporting Information

Controllable Synthesis of Two-Dimensional Ruddlesden-Popper Type Perovskite Heterostructures

Jun Wang[1#], Junze Li[1#], Qinghai Tan[2, 3], Lei Li[1], Jianbing Zhang[1], Jianfeng Zang[1, 4],

Pingheng Tan[2, 3], Jun Zhang[2, 3*] and Dehui Li[1, 5*]

[1]*School of Optical and Electronic Information, Huazhong University of Science and Technology, Wuhan, 430074, China;*
[2]*State Key Laboratory of Superlattices and Microstructures, Institute of Semiconductors, Chinese Academy of Sciences, Beijing 100083, China*
[3] *College of Materials Science and Opto-Electronic Technology, University of Chinese Academy of Sciences, Beijing 101408, China*
[4]*Innovation Institute, Huazhong University of Science and Technology, Wuhan, 430074, China;*
[5]*Wuhan National Laboratory for Optoelectronics, Huazhong University of Science and Technology, Wuhan, 430074, China;*

[#] Those authors contribute to this work equally.

*Correspondence to: Email: zhangjwill@semi.ac.cn; dehuili@hust.edu.cn.

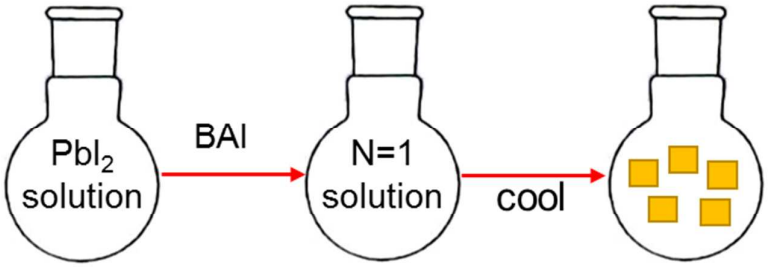

Figure S1. Schematic illustration of the solution process for obtaining centimeter-size N=1 2D perovskite. This procedure has been successfully used to synthesis relatively pure $(BA)_2MA_{N-1}Pb_NI_{3N+1}$ (N=1-5)[1, 2]. To obtain centimeter-size plates, the reaction temperature is 140 °C which is higher than the boiling point, and the saturation solution were kept static overnight.

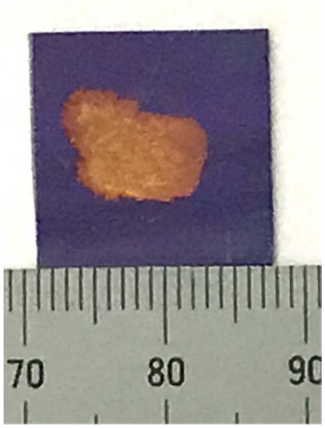

Figure S2. Backside view of vertical heterostructure shown in Fig. 1f in the maintext. The yellow color represents the color of N=1 2D perovskite, confirming the formation of the vertical heterostructure.

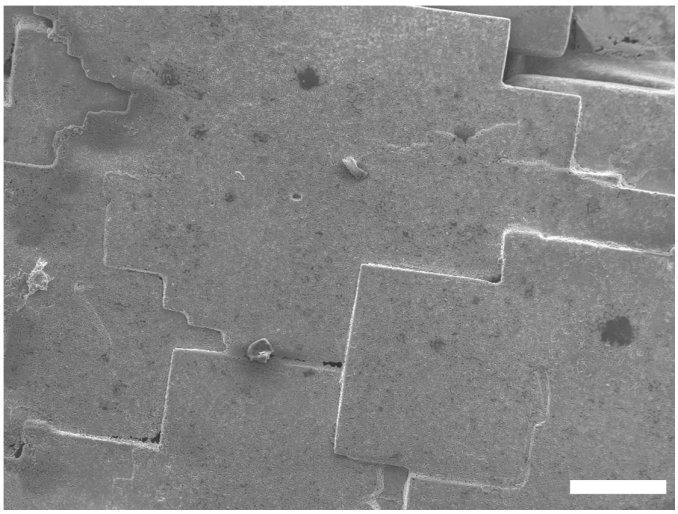

Figure S3. SEM image of N=1 plate obtained by solution process. The scale bar is 100 μm. The surface of N=1 plate before gas-solid phase intercalation process is relatively smooth.

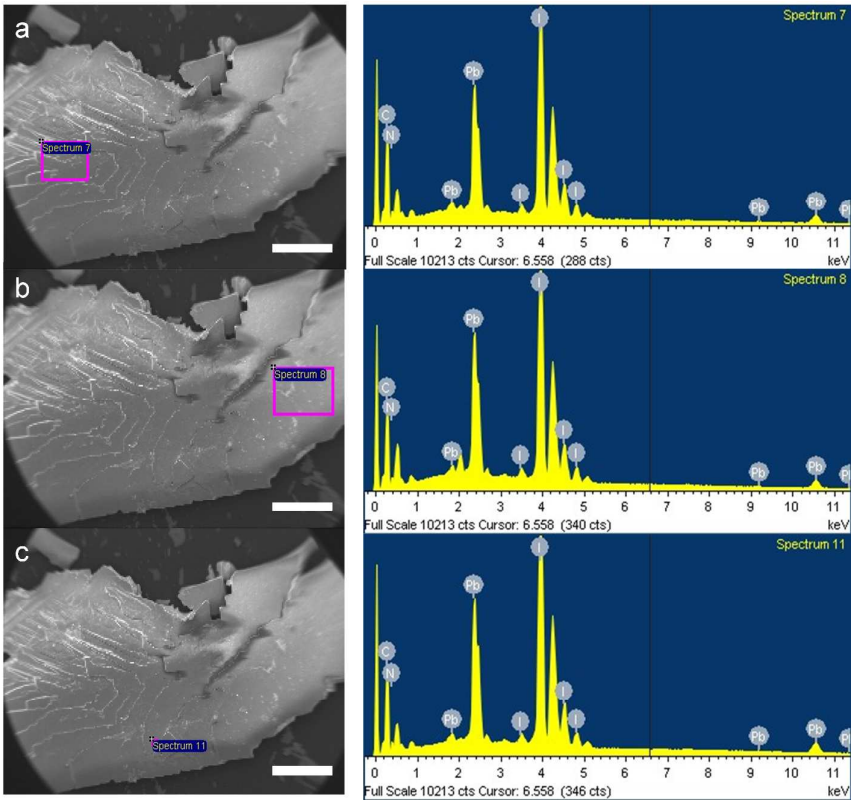

Figure S4. SEM-EDX images of lateral heterostructure for (a) N=1 portion (b) N=2 portion and (c) junction region. The scale bar is 2 mm. No Cl element was detected on the surface of the heterostructure even when MACl was used as precursor.

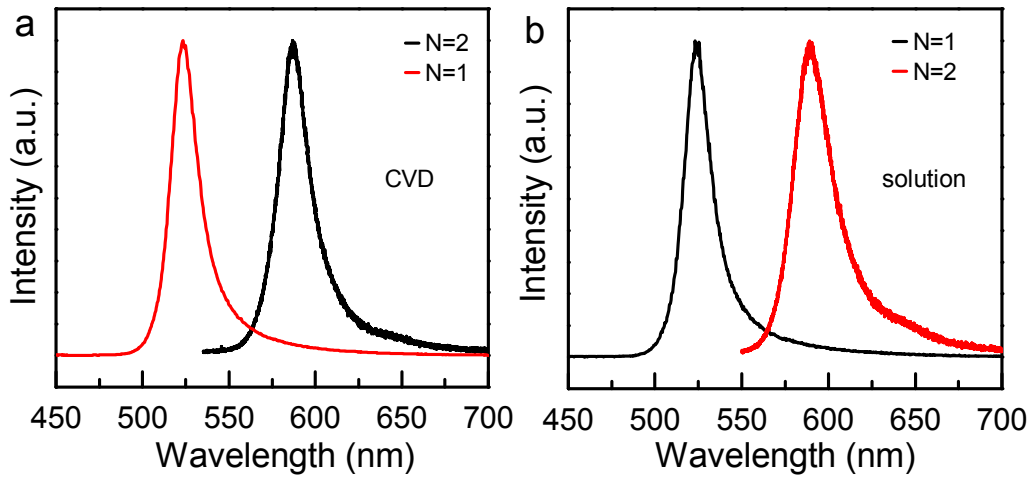

Figure S5. PL spectrum of N=1 and N=2 2D perovskite obtained by (a) gas-solid phase intercalation process and (b) solution method. The emission peaks of N=1 and N=2 portion of the lateral heterostructure coincide with those of N=1 and N=2 plates obtained by solution method, indicating that the low-temperature gas-solid intercalation preserves the crystal structures of N=1 and N=2 2D perovskites

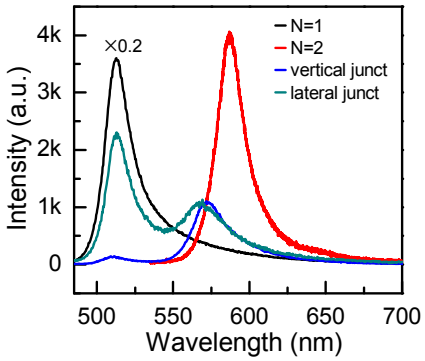

Figure S6. PL spectra show the intensity quenching for $(BA)_2PbI_4$/ $(BA)_2MAPb_2I_7$ lateral and vertical heterostructures. The emission intensity of the junction region for both lateral and vertical N=1/N=2 2D perovskite heterostructures significantly decreases compared with that of N=1 and N=2 regions. The charge transfer at the junction region might be a reason which has been found in other heterostructures[3, 4, 5].

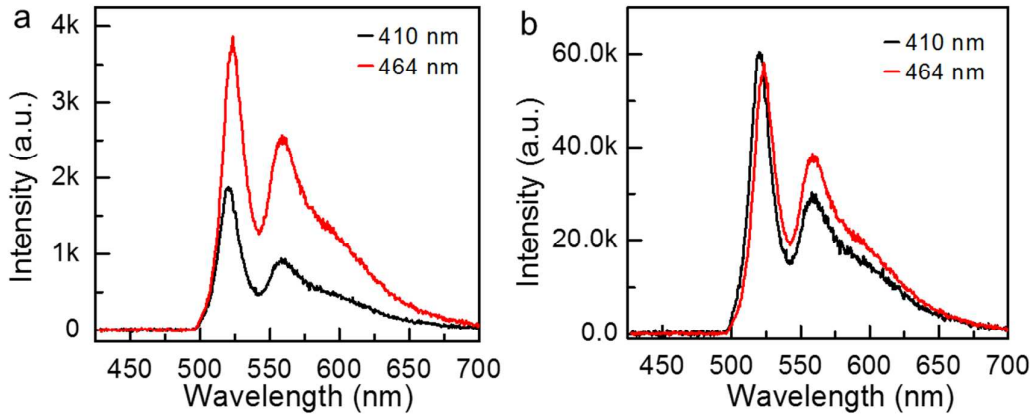

Figure S7. PL spectra excited at 410 nm and 460 nm for (a) vertical and (b) lateral heterostructures. For both lateral and vertical heterostructures, the excitation with higher energy leads to a blue-shift of the emission peak and relative stronger emission for N=1 compared with that of N=2.

.

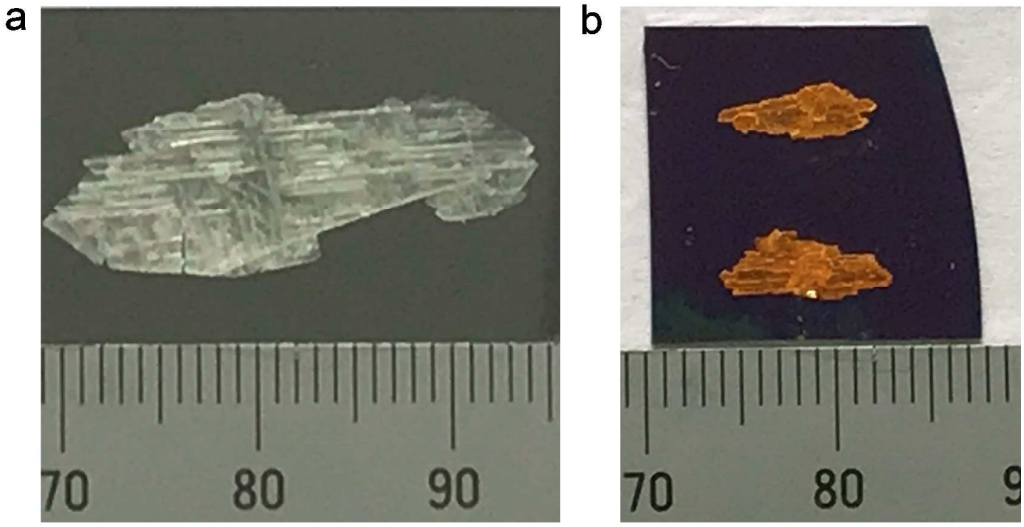

Figure S8. Picture of (a) $(BA)_2PbBr_4$ and (b) $(PEA)_2PbBr_4$ before intercalation. The synthesis of these two type 2D perovskites is similar to $(BA)_2PbI_4$ as shown in Supplementary Fig. 1. The centimeter size of the plates provides relatively easier procedure to obtain vertical and especially lateral heterostructures for which a piece of Si substrate was used as mask in our experiments

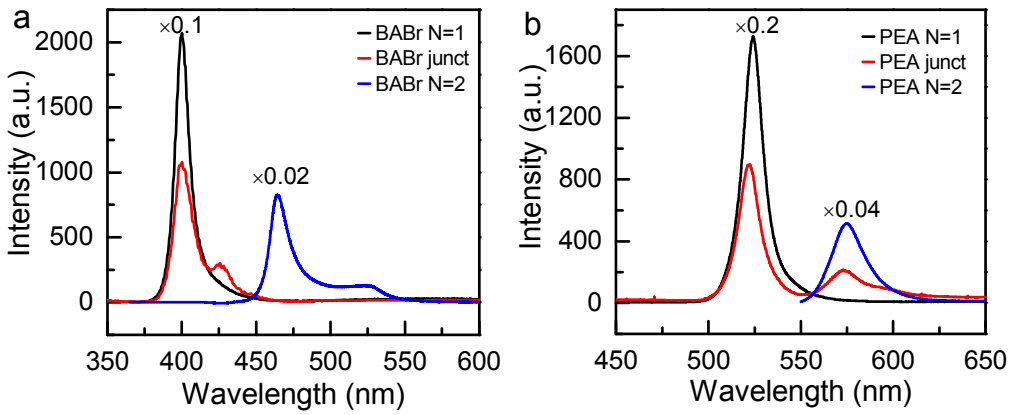

Figure S9. PL spectra show the intensity quenching for (a) $(BA)_2PbBr_4/(BA)_2MAPb_2Br_7$ and (b) $(PEA)_2PbI_4/(PEA)_2MAPb_2I_7$ lateral heterostructures compared with PL intensity acquired at N=1 and N=2 regions.

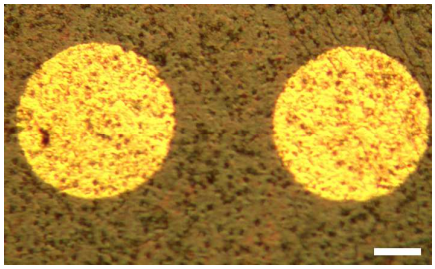

Figure S10. Optical image of a lateral heterojunction device. The scale bar is 50 μm. For lateral heterostructure device, two 5 nm Cr/50 nm Au electrodes were defined by shadow mask and e-beam evaporation, on a 300 nm SiO_2/Si substrate with a channel length of around 100 μm.

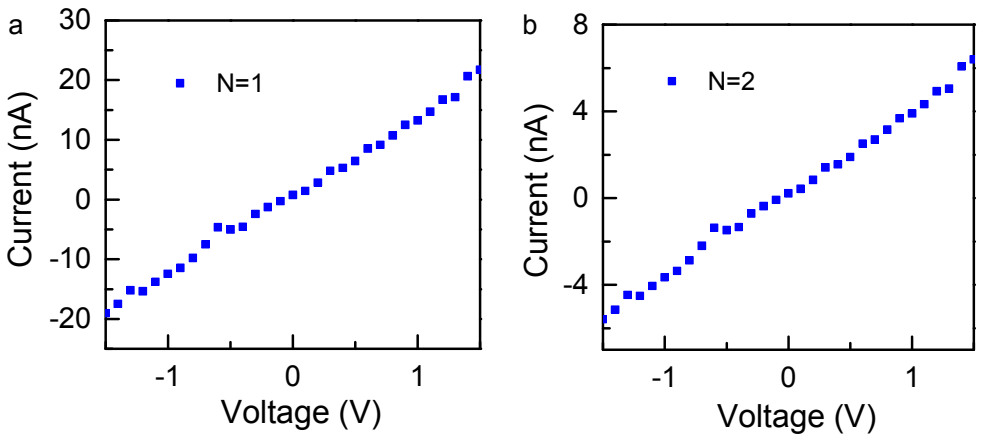

Figure S11. I-V curves for a) $(BA)_2PbI_4$ and b) $(BA)_2MAPb_2I_7$ 2D perovskite plates with Cr/Au electrical contact.

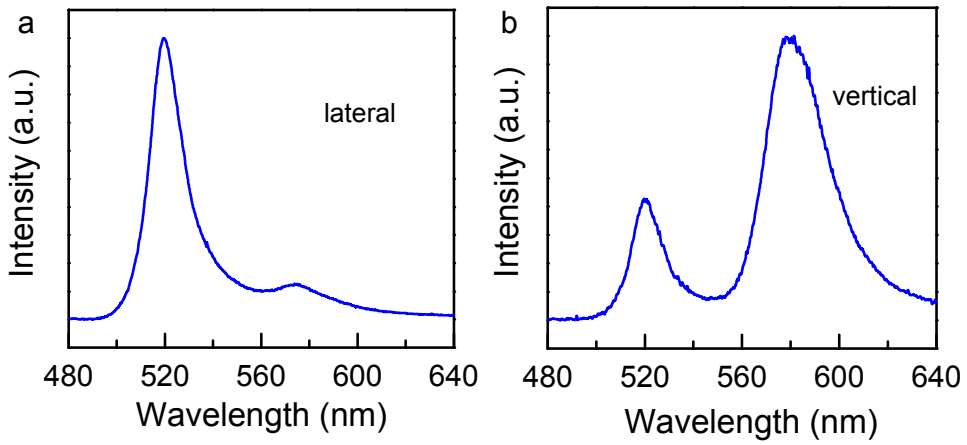

Figure S12. PL spectra from (a) lateral and (b) vertical devices.

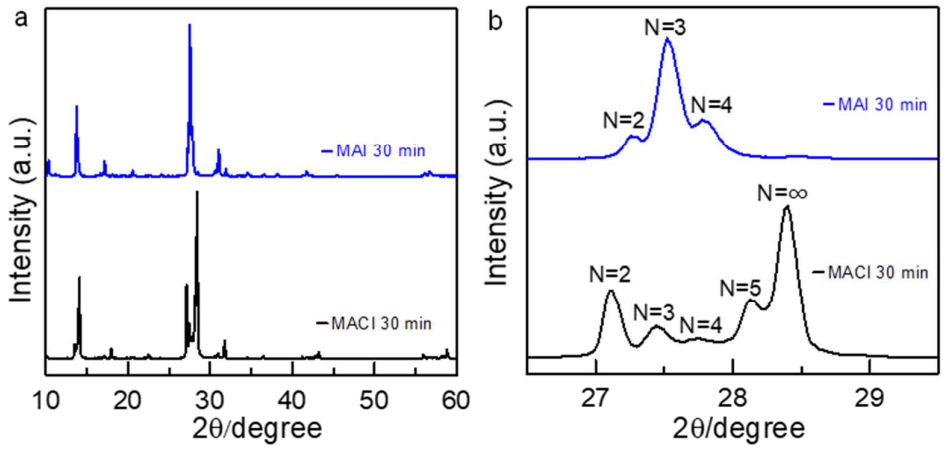

Figure S13. (a) XRD patterns of $(BA)_2(MA)_{N-1}Pb_NI_{3N+1}$ for MAI and MACl used as precursor. (b) Close-up views of the characteristic regions between 2θ = 26.5−29.5° show the different reaction ratios for MACl and MAI. The as-synthesized multi-heterostructure contains peaks from N=2 to N=4 and weak peak of N=∞ by using MAI as the precursor source while from N=2 to N=∞ by using MACl as the precursor in (b)[6, 7].

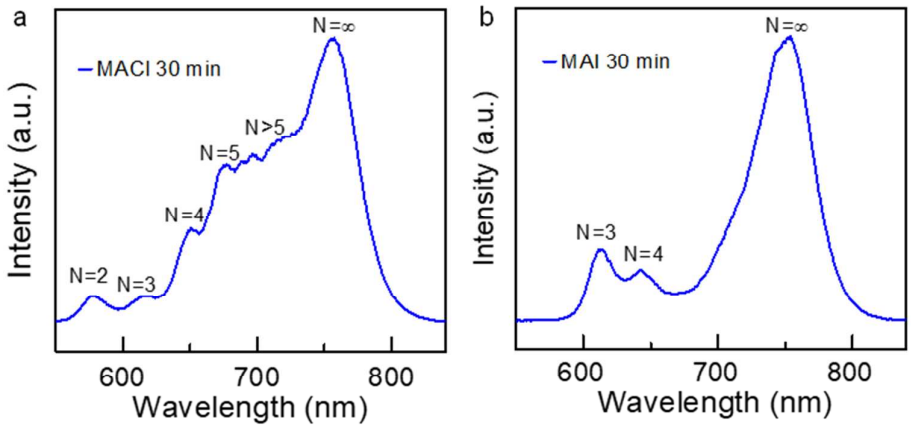

Figure S14. PL spectra from $(BA)_2(MA)_{N-1}Pb_NI_{3N+1}$ multi-heterostructures obtained by using(a) MACl and (b) MAI as precursors reacting for 30 min.

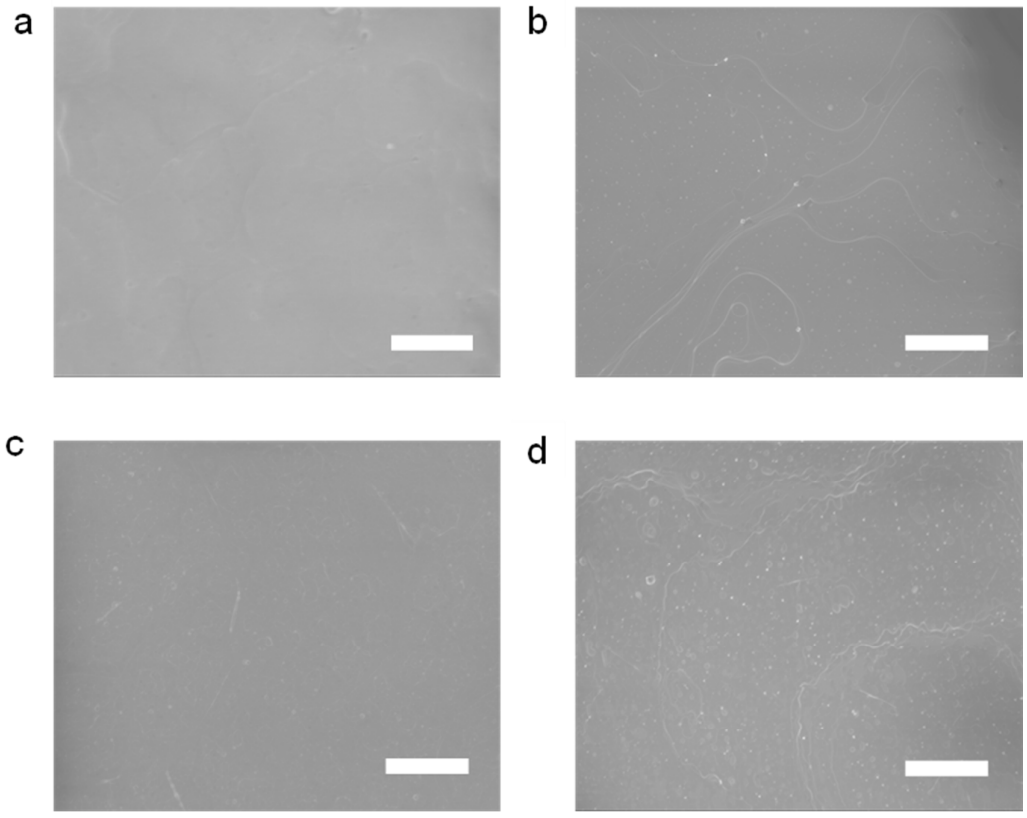

Figure S15. SEM image of lateral heterostructure after being stored in ambient conditions for a) pristine, b) 20 days, c) 40 days, d) 60 days. The scale bar is 20 μm. The surface of the heterostructure looks relatively smooth after 60 days.

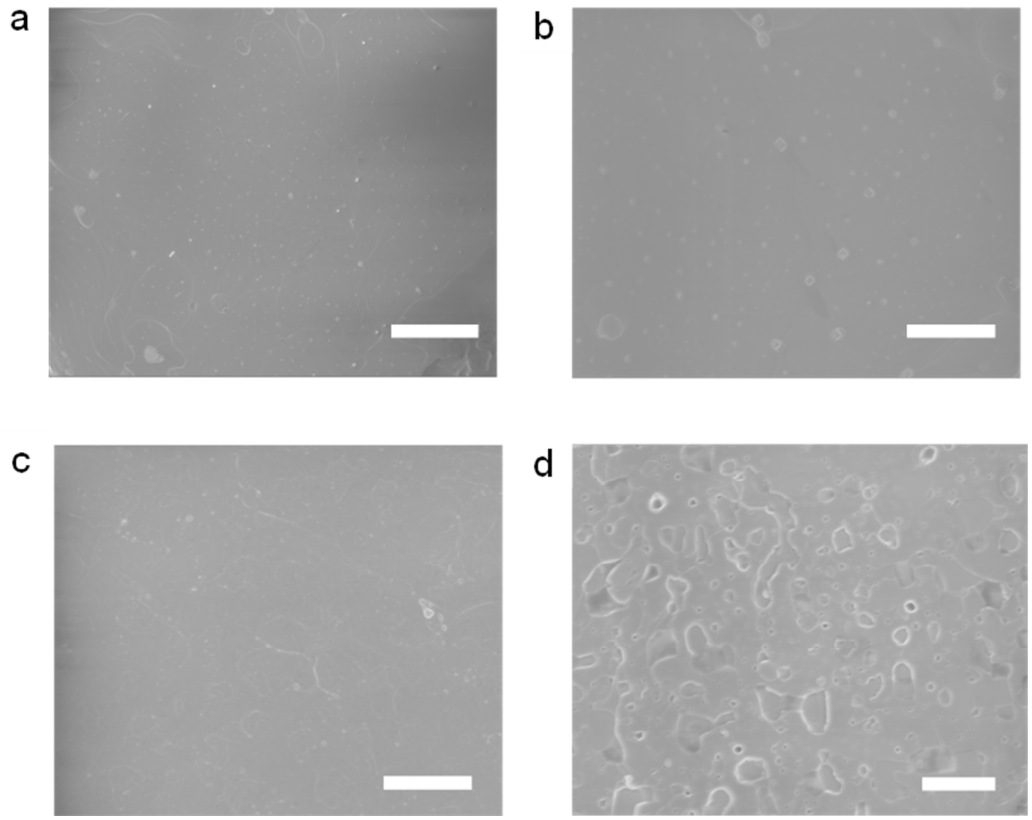

Figure S16. SEM image of vertical heterostructure after being stored in ambient conditions for a) pristine, b) 20 days, c) 40 days, d) 60 days. The scale bar is 20 μm. The surface of the heterostructure looks relatively smooth after 60 days.

	N=2 solution		N=2 lateral		N=2 vertical	
Element	Weight%	Atomic%	Weight%	Atomic%	Weight%	Atomic%
C	17.67	64.41	17.83	64.37	17.89	64.25
N	4.11	11.60	3.81	11.78	3.88	11.94
I	54.66	17.03	56.23	19.22	55.12	18.41
Pb	20.76	3.96	22.14	4.63	21.11	4.39

Table S1. Elements contained obtained by EDX for lateral heterostructure. The atomic ratio of the solution processed N=2 2D perovskite is consistent with that of N=2 portion in both lateral and vertical N=1/N=2 heterostructures produced by our gas-solid intercalation method, which further conforms the successful formation of N=1/N=2 heterostructures.

References

(1) Cao, D. H.; Stoumpos, C. C.; Farha, O. K.; Hupp, J. T; Kanatzidis, M. G. 2D homologous perovskites as light-absorbing materials for solar cell applications. *J. Am. Chem. Soc.* **2015,** *137*, 7843-7850.

(2) Blancon, J. C.; Tsai, H.; Nie, W.; Stoumpos, C. C.; Pedesseau, L.; Katan, C.; Kepenekian, M.; Soe, C. M. M.; Appavoo, K.; Sfeir, M. Y.; et al. Extremely efficient internal exciton dissociation through edge states in layered 2D perovskites. *Science* **2017,** *6331*, 1288.

(3) Wu, K., Chen, J.; McBride, J. R; Lian, T. Efficient hot-electron transfer by a plasmon-induced interfacial charge-transfer transition. *Science* **2015,** *349*, 632-635.

(4) Yuan, J.; Najmaei, S.; Zhang, Z.; Zhang, J.; Lei, S.; Ajayan, P. M.; Yakobson, B. I.; Lou, J. Photoluminescence quenching and charge transfer in artificial heterostacks of monolayer transition metal dichalcogenides and few-layer black phosphorus. *ACS Nano* **2015,** *9*, 555-563.

(5) Wang, H.; Bang, J.; Sun, Y.; Liang, L.; West, D.; Meunier, V.; Zhang, S. B. The role of collective motion in the ultrafast charge transfer in van der Waals heterostructures. *Nat. Commun.* **2016,** *7,* 11504.

(6) Stoumpos, C. C.; Cao, D. H.; Clark, D. J.; Young, J.; Rondinelli, J. M.; Jang, J. I.; Hupp, J. T.; Kanatzidis, M. G. Ruddlesden–Popper hybrid lead iodide perovskite 2D homologous semiconductors. *Chem. Mater.* **2016,** *28*, 2852-2867.

(7) Stoumpos, C. C.; Soe, C. M. M.; Tsai, H.; Nie, W.; Blancon, J.; Cao, D. H.; Liu, F.; Traore, B.; Katan, C.; Even, J.; Mohite, A. D.; Kanatzidis, M. G. High members of the 2D Ruddlesden-Popper halide perovskites: synthesis, optical properties, and solar cells of $(CH_3(CH_2)_3NH_3)_2(CH_3NH_3)_4Pb_5I_{16}$. *Chem.* **2017,** *2*, 427-440.